

Data Mining Inspired Localized Resistivity in Global MHD Simulations of the Magnetosphere

Harry Arnold¹, Kareem Sorathia², Grant K. Stephens³, Mikhail I. Sitnov⁴, Viacheslav G. Merkin², and Joachim Birn⁵

¹Johns Hopkins University Applied Physics Labs

²The Johns Hopkins University Applied Physics Laboratory

³Johns Hopkins University Applied Physics Laboratory

⁴JHU/APL

⁵SSI

November 23, 2022

Abstract

Recent advances in reconstructing Earth's magnetic field and associated currents by utilizing data mining of in situ magnetometer observations in the magnetosphere have proven remarkably accurate at reproducing observed ion diffusion regions. We investigate the effect of placing regions of localized resistivity in global simulations of the magnetosphere at specific locations inspired by the data mining results for the substorm occurring on July 6, 2017. When explicit resistivity is included, the simulation forms an x-line at the same time and location as the MMS observation of an ion diffusion region at 15:35 UT on that day. Without this explicit resistivity, reconnection forms later in the substorm and far too close to Earth ($\sim 15R_E$), a common problem with global simulations of Earth's magnetosphere. A consequence of reconnection taking place farther down the tail due to localized resistivity is that the reconnection outflows transport magnetic flux Earthward and thus prevent the current sheet from thinning enough for reconnection to take place nearer Earth. As these flows rebound tailward from the inner magnetosphere, they can temporarily and locally (in the dawn-dusk direction) stretch the magnetic field allowing for small scale x-lines to form in the near Earth region. Due to the narrow cross-tail extent of these x-lines ($\sim 5R_E$) and their short lifespan ($\sim 5\text{min}$), they would be difficult to observe with in situ measurements. Future work will explore time-dependent resistivity using 5 minute cadence data mining reconstructions.

Data Mining Inspired Localized Resistivity in Global MHD Simulations of the Magnetosphere

H. Arnold¹, K. Sorathia¹, G. Stephens¹, M. Sitnov¹, V.G. Merkin¹, J. Birn²

¹Johns Hopkins Applied Physics Laboratory, Laurel, MD USA

²Space Science Institute, Boulder, CO USA

Key Points:

- Localized Resistivity in global MHD simulations can “encourage” magnetic reconnection in specific locations to match data mining results
- Magnetic reconnection at $X_{GSM} \lesssim -20R_E$ can suppress the formation of extended x-lines at $X_{GSM} \gtrsim -15R_E$
- Reconnection outflows rebound from the near-Earth region causing transient and narrow (in Y_{GSM}) secondary reconnection

Corresponding author: Harry Arnold, harryarnold@jhuapl.edu

Abstract

Recent advances in reconstructing Earth’s magnetic field and associated currents by utilizing data mining of in situ magnetometer observations in the magnetosphere have proven remarkably accurate at reproducing observed ion diffusion regions. We investigate the effect of placing regions of localized resistivity in global simulations of the magnetosphere at specific locations inspired by the data mining results for the substorm occurring on July 6, 2017. When explicit resistivity is included, the simulation forms an x-line at the same time and location as the MMS observation of an ion diffusion region at 15:35 UT on that day. Without this explicit resistivity, reconnection forms later in the substorm and far too close to Earth ($\gtrsim -15R_E$), a common problem with global simulations of Earth’s magnetosphere. A consequence of reconnection taking place farther down the tail due to localized resistivity is that the reconnection outflows transport magnetic flux Earthward and thus prevent the current sheet from thinning enough for reconnection to take place nearer Earth. As these flows rebound tailward from the inner magnetosphere, they can temporarily and locally (in the dawn-dusk direction) stretch the magnetic field allowing for small scale x-lines to form in the near Earth region. Due to the narrow cross-tail extent of these x-lines ($\lesssim 5R_E$) and their short lifespan ($\lesssim 5\text{min}$), they would be difficult to observe with in situ measurements. Future work will explore time-dependent resistivity using 5 minute cadence data mining reconstructions.

Plain Language Summary

[enter your Plain Language Summary here or delete this section]

1 Introduction

Earth’s magnetosphere is a dynamic system driven by the solar wind. Magnetic reconnection on the day side transfers magnetic flux to the night side, gradually increasing the magnetic energy density in the tail lobes during the growth phase of a substorm. At some point the expansion phase is explosively triggered, likely due to demagnetization of ions (Schindler, 1974; Sitnov & Schindler, 2010; Sitnov et al., 2013; Bessho & Bhat-tacharjee, 2014; Pritchett, 2015) or electrons (Coppi et al., 1966; Hesse & Schindler, 2001; Liu et al., 2014), and the stored energy in the lobes is released through magnetic reconnection (Baker & P, 1996; Angelopoulos et al., 2008). This results in the dipolarization of the nightside magnetic field (Russell & McPherron, 1973).

Modelers have successfully simulated many of the observed features of substorms, including magnetotail reconnection and resulting dipolarization (e.g. Birn et al., 1996; Raeder, 2003; Merkin et al., 2019). However, no single simulation can correctly simulate all the physics due to the several orders of magnitude difference between kinetic and global scales. This has led to different efforts to understand the relevant physics, but there are still many questions unanswered. Notably, where and when does magnetic reconnection take place in the magnetotail and how does that affect the global system?

We investigate this question in the context of a global magnetohydrodynamic (MHD) simulation, but also consider the important role non-MHD effects play in determining the location and timing of reconnection in the magnetotail. Prior to reconnection onset, the tail current sheet may have a multiscale structure with an ion-scale thin current sheet embedded in a thicker plasma sheet (Sergeev et al., 2011) or it may be bifurcated on similar ion scales (Nakamura et al., 2002; Runov et al., 2003, 2005, 2006; Sergeev et al., 2003). While Birn and Schindler (2002) have demonstrated that thin current sheets can form even within a quasi-static isentropic model with isotropic pressure (equivalent to slow ideal MHD evolution), other approaches have indicated the possibly important role of pressure anisotropy (Artemyev et al., 2021). Further, during, or even prior to, reconnection the current sheet thins even more down to electron scales (Torbert et al., 2018).

62 Additionally, several studies indicate that x-lines are commonly expected and observed
 63 to be near $-40R_E < X_{GSM} < -20R_E$ (L. Q. Zhang et al., 2010; Nagai et al., 1998;
 64 Imber et al., 2022; Zhao et al., 2016). However, extended x-lines are often seen too close
 65 to the Earth in global MHD simulations (El-Alaoui et al., 2009; Gong et al., 2021; Bard
 66 & Dorelli, 2021; Park, 2021) (see also Fig. 3 (a)) and even in Hall MHD or hybrid sim-
 67 ulations (Bard & Dorelli, 2021; Runov et al., 2021).

68 Recently, data mining (DM) has been harnessed to reconstruct the state of the mag-
 69 netosphere for a given point in time (G. Stephens et al., 2019). In order to test the ac-
 70 curacy of this method the authors examined $B_{z,GSM} = 0$ contours in the magnetotail
 71 current sheet and compared them to Magnetospheric Multiscale Mission (MMS) obser-
 72 vations of ion diffusion regions (IDRs). Ions decouple from the magnetic field in IDRs
 73 and thus IDRs are useful for identifying features in the magnetic field geometry such as
 74 x- and o-lines. The authors were able to show these contours were within $1R_E$ of an MMS
 75 identified IDR for 16 out of 26 total IDRs. 8 others were within $1R_E$ of a $2nT$ contour,
 76 signifying that DM was close to resolving the reconnection site (G. K. Stephens et al.,
 77 2022). This is especially impressive since one of the misses occurred during a time of weak
 78 magnetospheric activity and the other was during a gap in solar wind data. By identi-
 79 fying the location of x-lines in the reconstruction and placing localized resistivity in these
 80 regions in the MHD simulation, we can effectively take non-MHD physics into account
 81 and “encourage” the simulation to form an x-line where and when we expect there to
 82 be reconnection from the DM results. Without this intervention the crucial process of
 83 tail reconnection will not occur at the correct time or location, which will affect the global
 84 response of the magnetosphere.

85 This paper presents results from different simulations that all model the substorm
 86 that took place on July 6, 2017 from approximately 15:35 to 17:00. We demonstrate that
 87 a localized resistivity can successfully induce reconnection in different locations in the
 88 tail. An unexpected result is that reconnection farther down the tail may actually sup-
 89 press near-Earth reconnection by transporting magnetic flux there and preventing the
 90 current sheet from collapsing. However, due to the 3D nature of the tail, the magnetic
 91 field can be stretched again by rebounding flows resulting in smaller, transient x-lines
 92 in the near-Earth region. These rebounding flows are a well known feature observation-
 93 ally (e.g. Ohtani et al., 2009) and have been found in global simulations as well (e.g. Merkin
 94 et al., 2019). However, the additional reconnection they can create has not yet been dis-
 95 cussed.

96 In section 2 we describe the simulations that we examine and the methodology for
 97 identifying x-lines in our simulations. In section 3 we show that DM inspired localized
 98 resistivity can create x-lines that match observations. In section 4 we explain how re-
 99 connection farther in the tail suppresses extended x-line near Earth. In section 5 we present
 100 evidence of small x-lines that form in rebounding flows. And in section 6 we conclude.

101 2 Event Description and Simulation Setup

102 We perform simulations using the global magnetohydrodynamic code GAMERA
 103 (B. Zhang et al., 2019; Sorathia et al., 2020) coupled with the ionospheric potential solver
 104 REMIX (Merkin & Lyon, 2010), which used a constant conductance of $5S$. Our simu-
 105 lations consist of a distorted spherical grid and a cylinder as the boundary with the faces
 106 located at $X_{SM} = 30R_E$ and $X_{SM} = -330R_E$. The radius of the cylinder is $110R_E$
 107 and it consists of $96 \times 96 \times 128$ grid cells in the radial, polar, and azimuthal dimensions re-
 108 spectively. This leads to a grid cell of length $\sim 0.5R_E$ at $X_{GSM} = -20R_E$. The mag-
 109 netosphere is driven using data from the OMNI database for the period on July 6, 2017
 110 from 14:35-17:35. The Sym-H magnitude remained small for the entirety of the simu-
 111 lation indicating that the ring current is not important to magnetospheric dynamics. Prior
 112 to the simulation, there is a spin-up period of two hours where a dipole magnetosphere

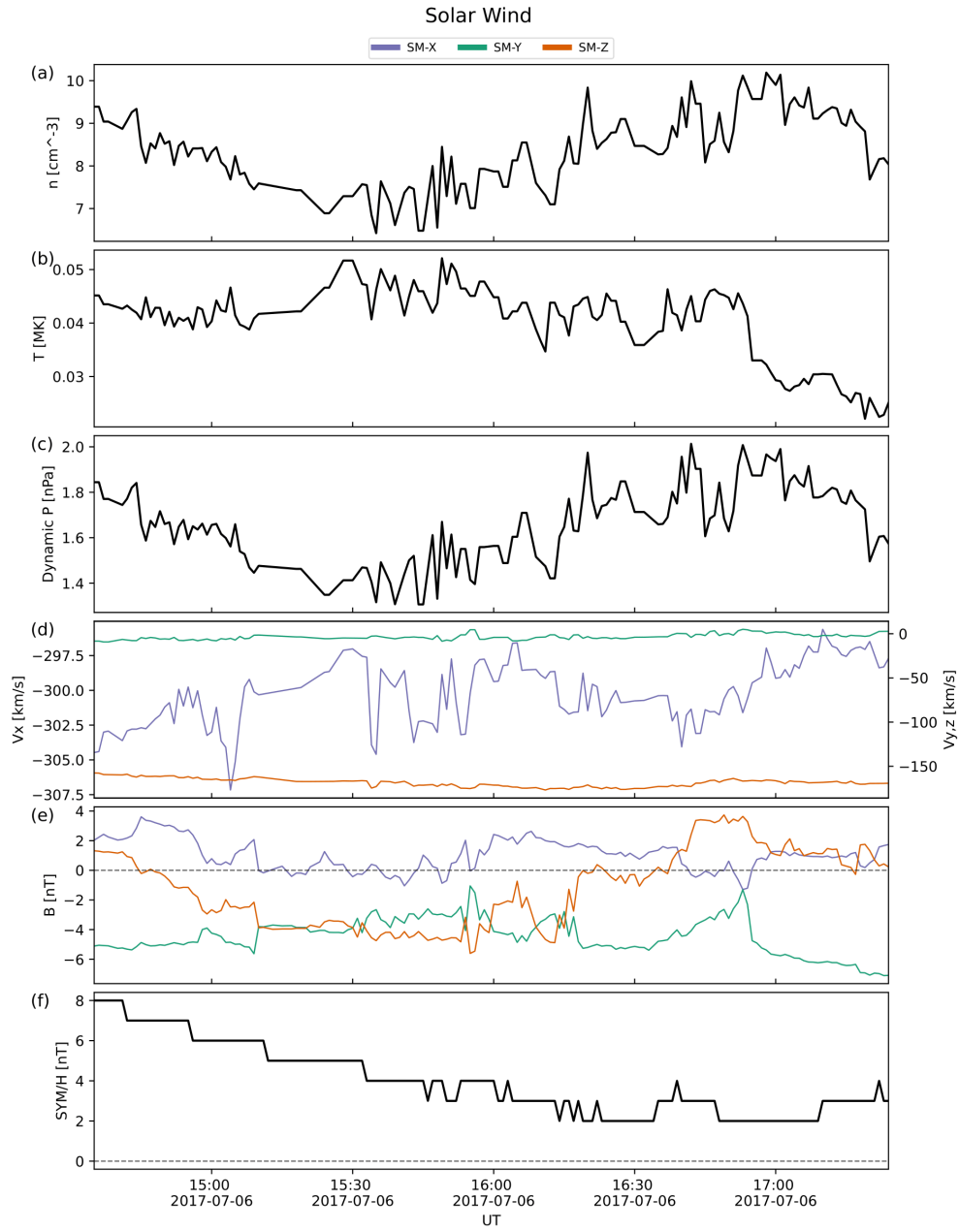


Figure 1. Solar wind parameters from the National Aeronautics and Space Administration OMNI database for the period of our simulations. (a) density, (b) temperature, (c) dynamic pressure, (d) flow velocity, (e) magnetic field, and (f) SYM-H index. The vector quantities are in Solar Magnetic Coordinates.

113 is driven by a hydrodynamic solar wind corresponding to the initial values on the left
 114 side of Fig. 1. All of our simulations result in substorm dynamics due to the southward
 115 turning IMF magnetic field.

In this paper we examine 3 simulations: one with no explicit resistivity (Run Base), one with localized resistivity placed near $X_{GSM} \sim -30R_E$ (Run Mid) and one with localized resistivity placed at a location inspired from DM results (Run DM). The location is specified by X_{SM} , Y_{SM} , and Z_{SM} coordinates with varying widths in each direction. The resistivity in our simulations is defined as

$$\eta = \eta_0 / \cosh^2\left(\frac{x - x_0}{L_x} + \frac{y - y_0}{L_y} + \frac{z - z_0}{L_z}\right) \quad (1)$$

116 where x_0 , y_0 , and z_0 give the center of the resistive region in SM coordinates, $\eta_0 = 40,000\Omega m$
 117 as in (Hesse & Birn, 1994), $L_x, L_y, L_z = 5, 20, 25R_E$ for Run Mid, and $L_x, L_y, L_z =$
 118 $6, 10, 4R_E$ for Run DM. Calculating the relevant scales from Run Mid in the resistive re-
 119 gion, we find a length of $\sim 1R_E$ for the width of the current sheet in the Z_{GSM} direc-
 120 tion, and a characteristic upstream Alfvén speed of $\sim 1000km/s$ which gives a Lundquist
 121 number of $S = LU\mu_0/\eta \sim 200$ where μ_0 is vacuum permeability. We also decreased
 122 this value of resistivity in a separate simulation (not shown) by an order of magnitude,
 123 and in that case the localized region of resistivity was unable to lead to substantial re-
 124 connection.

125 In order to explore the effects of resistivity, we developed a method to identify the
 126 location of x-lines. Since we are primarily interested in tail reconnection, we limited our-
 127 selves to the region $-60 < X_{GSM}/R_E < -5$, $-10 < Y_{GSM}/R_E < 10$, and $-10 <$
 128 $Z_{GSM}/R_E < 10$. Further, we required that the azimuthal current (in GSM coordinates)
 129 be larger than $\sim 0.5A/m^2$ and that both $B_{Z,GSM}$ and $B_{X,GSM}$ reverse sign within 1
 130 grid cell of the suspected x-line location. Then we trace the magnetic field lines for $3R_E$
 131 in the $X_{GSM}-Z_{GSM}$ plane, both parallel and anti-parallel to \mathbf{B} , starting at $X_{GSM} \pm$
 132 $1R_E$ from the identified cell. The result is 4 different locations where both ends of the
 133 field line that started on the Earthward side of the cell in question will remain on the
 134 Earthward side and similarly for the tailward side if the identified cell is an x-line. How-
 135 ever, we only require 3 of the final locations to follow this pattern as the reconnecting
 136 magnetic field is not guaranteed to perfectly lie along X_{GSM} . The resulting identified
 137 x-lines have been verified to have a general agreement with the expected geometry. How-
 138 ever, they tend to be spread out in the X_{GSM} and Y_{GSM} directions in the vicinity of an
 139 x-line which introduces some unavoidable error.

140 3 Localized Resistivity Induces Reconnection

141 There have been many studies of the magnetotail with resistive MHD simulations,
 142 and in particular MHD simulations with localized patches of resistivity (Hesse & Birn,
 143 1994; Raeder et al., 1996; Raeder, 1999; Raeder et al., 2001; Birn & Hesse, 2013). These
 144 have shown that a localized region of resistivity can induce reconnection locally (Ugai
 145 & Tsuda, 1979; Min et al., 1985; Scholer & Otto, 1991). However, until now there has
 146 been no way to inform the simulation about where and when reconnection should take
 147 place in the magnetotail. Using the magnetosphere reconstruction results from DM, we
 148 can determine the location of reconnection with reasonable accuracy. And by strategi-
 149 cally placing localized resistivity we will be able to induce reconnection that approxi-
 150 mately matches both the spatial and temporal profiles of real x-lines in a given substorm accord-
 151 ing to DM reconstructions.

152 As a first step we looked at the x-line that was identified by the MMS on July 6,
 153 2017 at $[X_{GSM}, Y_{GSM}, Z_{GSM}] = [-24.1, 1.41, 4.44]R_E$ (Rogers et al., 2019). In order
 154 to match the location of the observed x-line, we placed a region of resistivity as described
 155 above to induce reconnection in the appropriate place as determined from DM. The com-
 156 parison with the simulation without resistivity as well as the DM results can be seen in

157 Fig. 2. Panel (a) shows the DM results in the $X'_{GSM}-Z_{GSM}$ plane, (b) is the DM re-
 158 sults in the $X_{GSM}-Y_{GSM}$ plane, (c) is at the same time but from Run Base in the $X_{GSM}-$
 159 Z_{GSM} plane, (d) is in the $X_{GSM}-Y_{GSM}$ plane, and (e)-(f) are the same as (c)-(d) but
 160 from Run DM. The result is a significant difference in the development of the magne-
 161 tosphere. While both simulations form an x-line deep in the tail near $X_{GSM} \sim -40R_E$
 162 on the dawn side, only the simulation with a localized resistivity leads to reconnection
 163 geometry with outflows near $\sim -25R_E$ in excellent agreement with in situ observations.

164 4 Mid-Tail Reconnection Suppresses Near Earth Reconnection

165 The above demonstrates that we can induce reconnection with localized resistiv-
 166 ity. In the previous section we showed that we can match observations of ion diffusion
 167 regions with x-lines in a simulation at the correct place and time. However, to consider
 168 a more generalized case, we also look at a simulation with resistivity located in the re-
 169 gion $X_{GSM} \sim -30R_E$, Run Mid. This is because of observations suggesting this as the
 170 likely location of near Earth reconnection (Imber et al., 2022; Zhao et al., 2016) as well
 171 as the consistent and extended x-lines that the DM results suggest exist here (G. K. Stephens
 172 et al., 2022), thus Run Mid is also inspired by DM results. A snapshot of Run Base com-
 173 pared with Run Mid and Run DM can be seen in Fig. 3. An important consequence is
 174 that the resistivity induced reconnection in both Run Dm and Run Mid creates diverg-
 175 ing flows sooner. The Earthward flow transports flux to the near Earth region which pre-
 176 vents the current sheet from narrowing and thus suppresses near Earth reconnection that
 177 would otherwise take place. This is especially evident in Run Mid, but even in Run DM
 178 the x-lines are generally deeper in the tail. This process is what dipolarizes the inner mag-
 179 netosphere and naturally prevents reconnection there.

180 Without explicit resistivity any reconnection in this region (near $X_{GSM} \lesssim -30R_E$)
 181 is unsteady and is not extended along the dawn-dusk region. Fig. 4 illustrates this point
 182 quite clearly. To form this figure we group all identified x-lines within $2R_E$ of each other,
 183 take the average X_{GSM} location, calculate the extent in the dawn dusk direction as the
 184 width, and the center in the dawn dusk direction as the Y_{GSM} location. Thus each “x”
 185 is colored according to its Y_{GSM} location, plotted according to the time it occurred and
 186 its X_{GSM} location, and the size illustrates its width. We show the results for all three
 187 simulations. Finally, the observed AL index is also plotted for reference. Interestingly,
 188 all simulations form x-lines in the midtail region (near $X_{GSM} \sim -30R_E$) before the sub-
 189 storm onset. However, in Run Base and Run DM the x-lines are smaller in width, tend
 190 to drift tailward, and seemingly jump around in X_{GSM} . Shortly after the growth phase
 191 begins, an extended x-line forms in the near Earth region for Run Base, initially on the
 192 dusk side, and gradually retreats in the expansion phase.

193 For Run DM the resistivity induces reconnection on the dusk side near $X_{GSM} \sim$
 194 $-20R_E$ just before the start of the growth phase. As the substorm progresses, the x-line
 195 gradually extends farther and farther towards the dawn until it occupies most of the tail
 196 as can be seen in Fig. 3 (d). This stretching of the x-line is also why the x-line appears
 197 to approach Earth. In fact, the x-line on the dusk side stays within the region of resis-
 198 tivity at $X_{GSM} \sim -20R_E$, but approaches Earth on the dawn side. Note that even though
 199 the average X_{GSM} position approaches Earth, it still generally stays farther in the tail
 200 than in Run Base, especially near the midnight line and duskward as can be seen in Fig.
 201 3. The x-line then retreats and eventually breaks up in the the recovery phase.

202 By placing resistivity farther in the tail we initially see a similar result. The x-line
 203 forms, but then extends in the dawn dusk direction, and stays roughly constant well into
 204 the expansion phase. While this x-line stays roughly centered on the midnight line, it
 205 extends well into both the dawn and dusk sides. It is likely that the x-line is matching
 206 the region of resistivity as expected. Near the recovery phase the x-line finally begins
 207 to breakup before effectively disappearing altogether.

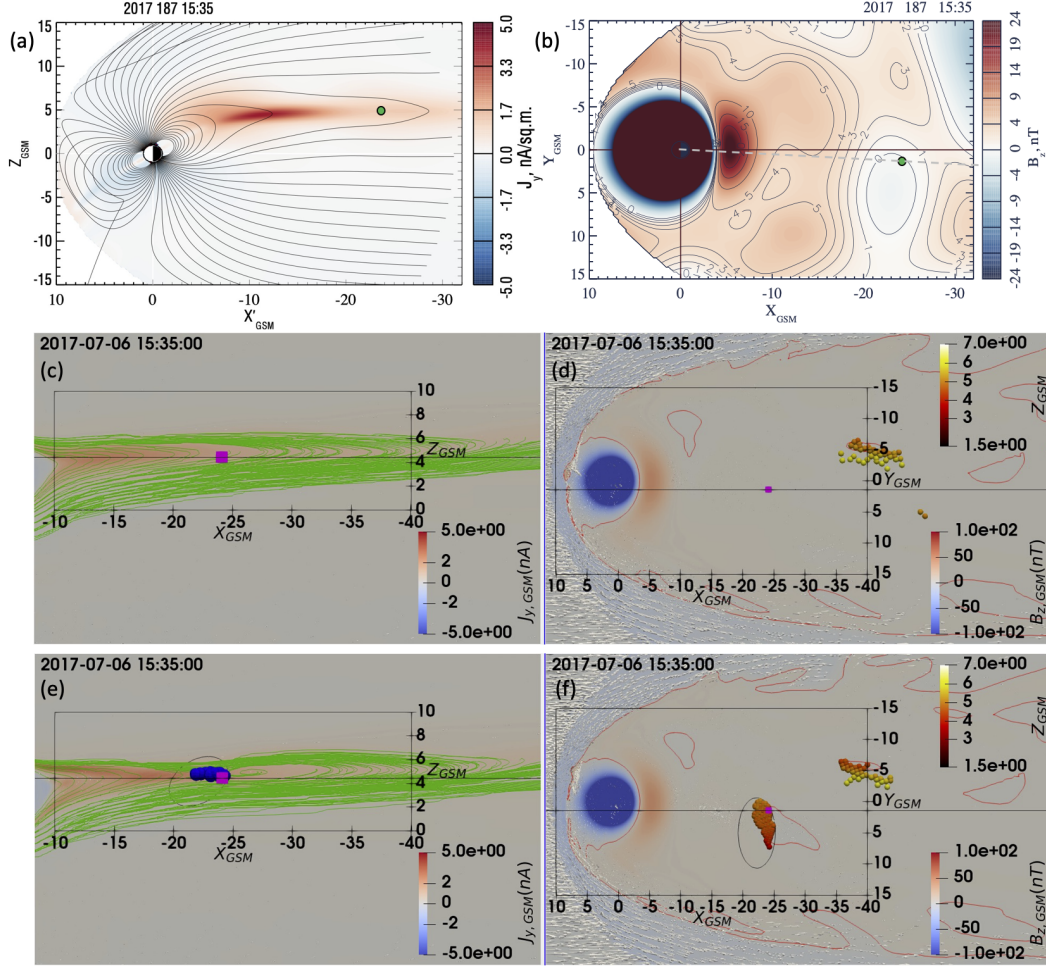


Figure 2. Each figure corresponds to July 6, 2017 at 15:35. Panel (a) and (b) show the DM reconstruction of the magnetosphere in the $X'_{GSM} - Z_{GSM}$ and $X_{GSM} - Y_{GSM}$ ($Z_{GSM} = 4.2R_E$) planes respectively. (a) is the current in the Y_{GSM} direction with field lines in black. (b) is $B_{Z,GSM}$ with contours equal to $B_{Z,GSM} = 0, 2, 3$ and $4nT$. The location of MMS is depicted by a green circle in both panels where it observed an ion diffusion region. The dashed line in (b) shows the location of the plane of (a) and the X'_{GSM} axis. Panels (c) and (d) are the $X_{GSM} - Z_{GSM}$ and $X_{GSM} - Y_{GSM}$ plane respectively from Run Base. (c) shows $J_{Y,GSM}$ with selected field lines in green, and (d) shows $B_{Z,GSM}$ with contours of $B_{Z,GSM} = 0$ in red. Both panels show flow vectors as white arrows. The horizontal lines in each plane corresponds to the location of the plane in the other panel. The pink squares are the location of MMS. The circles are the location of identified x-lines in the simulation, in (d) and (f) they are colored according to their Z_{GSM} location. (c) and (e) only show identified x-lines within $1R_E$ of the plane. Panels (e) and (f) are the same as (c) and (d) respectively except for Run DM. The black circles correspond to contours of resistivity equal to $10,000\Omega m$.

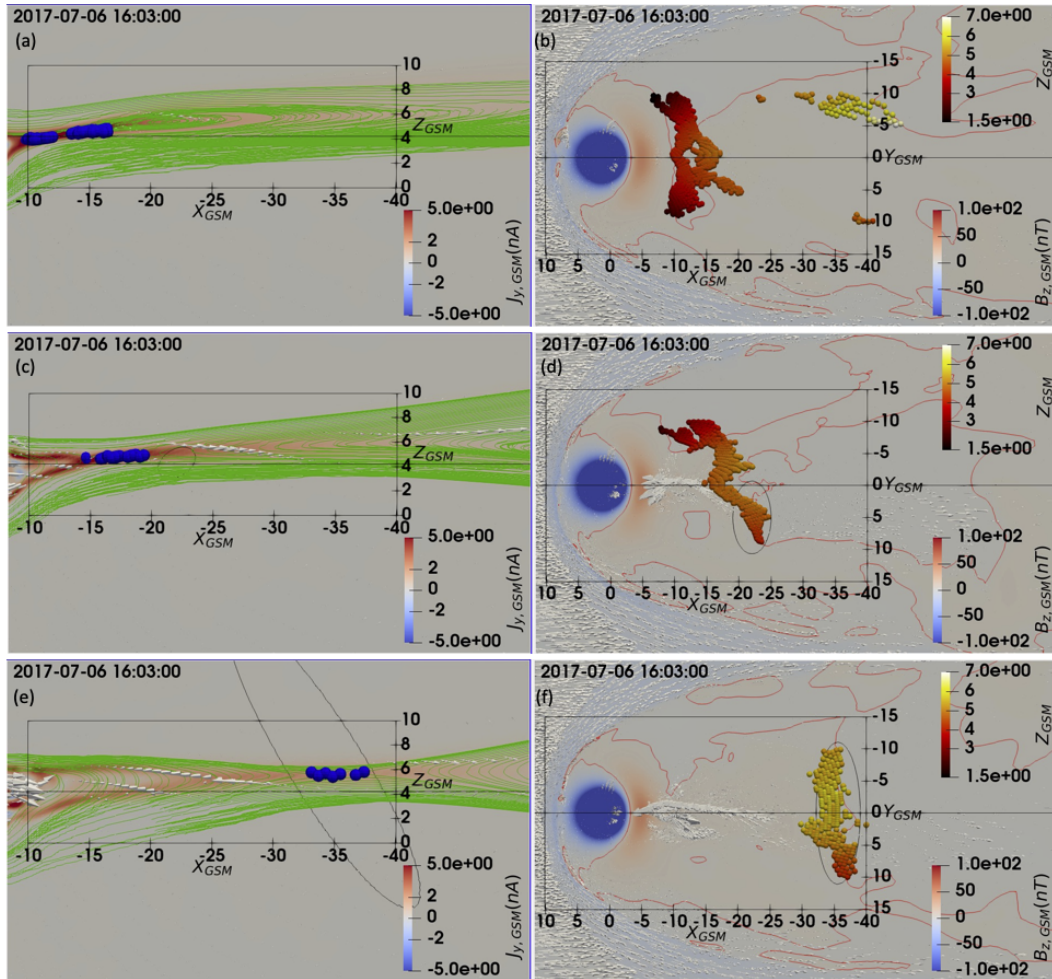


Figure 3. Each pair of panels in this figure have the same format as Fig. 2 (c)-(d). However, they are at a time shortly after reconnection begins in Run Base and they lack the location of MMS. (a) and (b) are from Run Base, (c) and (d) are from Run DM and (e) and (f) are from Run Mid.

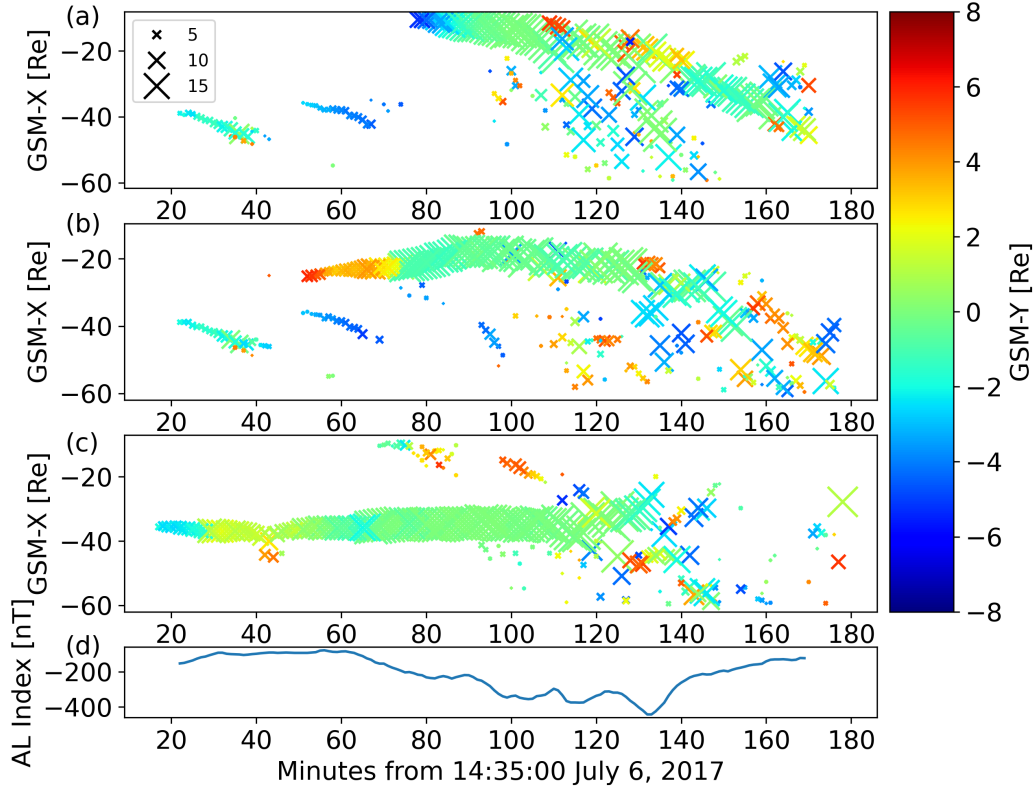


Figure 4. Panel (a) shows the x-lines seen throughout Run Base. Each “x” represents all identified x-lines within $2R_E$ of each other. The legend relates the size of each “x” to the width in the dawn-dusk direction in R_E . The color indicates the center of the x-line in the dawn-dusk direction. Panels (b) and (c) are the same as (a) but for Run DM and Run Mid respectively. Panel (d) is the observed AL index during this time period.

5 Rebounding Flows Stretch the Tail and Create Secondary X-Lines

The previous section clearly described how reconnection farther in the tail suppresses reconnection closer to Earth. However, as can be seen in Fig. 4 (c) there are some near Earth x-lines. These x-lines differ qualitatively from the near Earth x-lines in Run Base. Crucially, these x-lines do not last as long nor do they spread as far in the dawn-dusk direction. Additionally, they tend to form in rebounding flows. Rebounding flows are Earthward flows from reconnection that rebound tailward due to the strong magnetic field near Earth (Ohtani et al., 2009).

As an example of one of these x-lines in Run Mid consider Fig. 5. Panels (a) and (b) are similar to Fig. 3 (c) and (d) but zoomed in and at a different time. This is taken right after the x-line forms and clearly demonstrates that it forms in the tailward flow region as the reconnection outflow rebounds near Earth. Panels (c)-(f) depict various quantities as measured at one of the actual positions that the x-line forms, $[x, y, z] = [-11.05, .5, 4.31]$. However, since the x-line is tilted with respect to the x-axis as can be seen in panel (a), we define $B_{x,r}$ and $B_{z,r}$ to be the reconnecting and reconnected component of the magnetic field respectively. The vertical red dashed line indicates when the flow switches from Earthward to tailward and the vertical green line indicates when reconnection is observed. Shortly after the flow turns tailward the field lines continue to stretch as can be seen in the reduction of $B_{z,r}$ leading to secondary reconnection. These secondary x-lines were also observed in Run DM as can be seen by the small red “x”s in Fig. 4 (b). This suggests that this secondary reconnection may be a common consequence of midtail reconnection.

6 Conclusion

In this paper we have demonstrated the ability to induce reconnection in a global simulation of Earth’s magnetosphere. We did not address the physics of why and how reconnection was initiated at a particular location but rather imposed localized resistivity as a means to initiate it in agreement with in situ observations of MMS. This is an important first step towards incorporating real observations into simulations to study a more accurate depiction of substorms. With the DM results we can determine places where x-lines actually form during a substorm and place time dependent patches of local resistivity to induce reconnection at correct locations in a global simulation. This is important since global simulations, and in particular MHD simulations, are missing key kinetic physics which play an important role in determining the specifics of reconnection. However, the recent results demonstrating the accuracy of DM based reconstructions of the magnetosphere allow us to implicitly incorporate otherwise missing physics and correctly simulate the location of reconnection for a given substorm. Future work will include incorporating the time dependent motion of x-lines into our global simulation model.

Without any explicit resistivity, an extended x-line often forms far too close to Earth than we would expect (El-Alaoui et al., 2009; Gong et al., 2021; Bard & Dorelli, 2021; Park, 2021; Runov et al., 2021). This is a common problem in global simulations of the magnetosphere. Interestingly, by placing resistivity farther in the tail and inducing reconnection there, we implicitly suppress reconnection near Earth. This can be explained simply by noting that reconnection farther in the tail will dipolarize the near Earth magnetic field by transporting magnetic flux towards Earth and thus broaden the current sheet and prevent reconnection. There are no extended x-lines in the near Earth region for Run Mid, which is consistent with observations of most substorms.

A crucial caveat to this conclusion is that we expect smaller scale and shorter lived x-lines to appear in regions with a tailward flow. As the reconnection exhaust from the primary x-line in the midtail region reaches the stronger magnetic field near Earth and

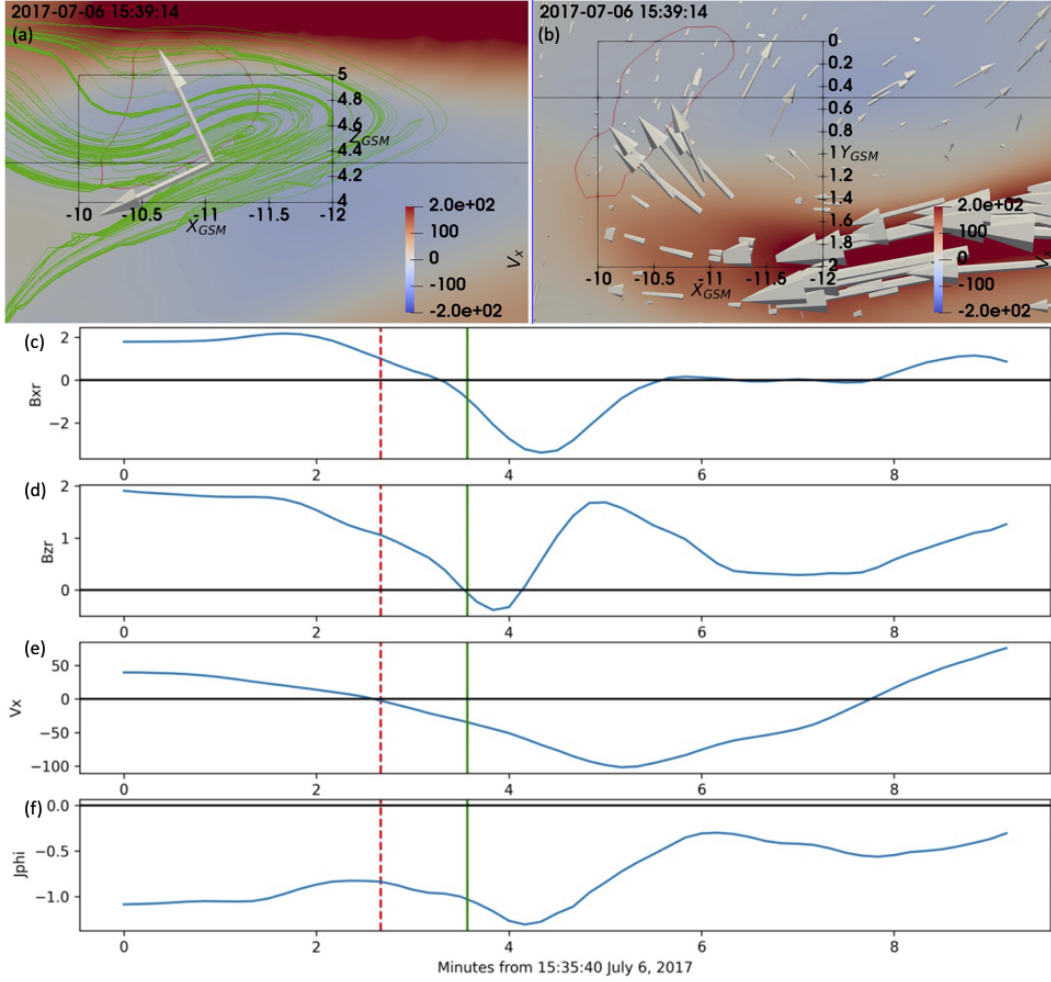


Figure 5. Panels (a) and (b) are similar to Fig. 3 (c) and (d) but zoomed in to show a near Earth x-line at an earlier time. The two tilted axes in panel (a) illustrate the “reconnection” axes for this x-line. Panels (c)-(f) show the reconnecting field ($B_{x,r}$), the reconnected field ($B_{z,r}$), $V_{X,GSM}$, and the azimuthal current in the GSM coordinate system, respectively. These quantities are plotted vs time for the position of the x-line as indicated by the origin of the “reconnection” axes ($[x, y, z] = [-11.05, 0.5, 4.31]$). The horizontal black line shows 0 for each quantity, the vertical red dashed line marks the switch from Earthward to tailward flow, and the vertical green line marks when reconnection is observed.

rebounds tailward, the magnetic field is stretched due to the frozen in condition. This stretching of the magnetic field is highly localized in the dawn-dusk direction, limited to $\sim 5R_E$ at most, and it can create x-lines that last on the order of ~ 10 minutes. Thin current sheets have been observed as part of the rebounding process (Panov et al., 2010; ?, ?) and they could lead to reconnection in a similar manner. However, to the authors' knowledge, these x-lines have not been directly observed. Due to their small nature both in time and space it would be rare for a satellite to obtain in situ measurements showing these x-lines. If these x-lines do form near Earth, they could play an important role in the production of energetic particles. As argued by Angelopoulos et al. (2020), the average energy per particle is much higher closer to Earth than it is where typical x-lines form due to the X_{GSM} dependence of the magnetic field strength. Thus even small scale x-lines could potentially create very energetic particles. This topic will also need to be explored with test particles in a future paper

Note that both near-mid tail X-lines (Run DM) and midtail X-lines (Run Mid) are observed in the DM analysis of substorms (Stephens et al., 2022). In our future simulations we plan to use the DM output with 5-min cadence to incorporate the whole empirical story of X-lines into Gamera simulations. Further efforts will be necessary to also reproduce the multiscale non-MHD structure of the tail current sheet prior to reconnection onsets.

Appendix A Average flows in near Earth secondary x-lines

Fig. A1 shows the maximum (red), average (black), and minimum (blue) velocity in the X_{GSM} direction for each group of x-lines identified in Run Mid that is closer than $20R_E$ in the tail to Earth. Note, that the average velocity of all these x-lines is $\sim -17m/s$. It is important to keep in mind that if the x-lines form in rebounding flows they will be close to the Earthward flow as can be seen in Fig. 3 (d). Since the x-line identification method inherently overestimates the area the x-line occupies we can naturally expect some of the identified "x-lines" to be in the Earthward flow. This explains why the maximum velocity is often Earthward if the x-line forms in tailward flows. However, the average velocity is typically negative further confirming that the x-lines do form in tailward flows.

Appendix B Open Research

The data used in the study are archived on Zenodo (<http://doi.org/10.5281/zenodo.7057795>).

Acknowledgments

This work was funded by NASA grants 80NSSC20K1271 and 80NSSC20K1787, as well as the NSF grant AGS-1744269. We also acknowledge support from the NASA DRIVE Center, Center for Geospace Storms. Joachim Birn acknowledges support by NASA grant 80NSSC18K0834.

References

- Angelopoulos, V., Artemyev, A., Phan, T. D., & Miyashita, Y. (2020). Near-earth magnetotail reconnection powers space storms. *Nature Physics*, *16*, 317-321.
- Angelopoulos, V., McFadden, J., Larson, D., Carlson, C. W., Mende, S., Frey, H., . . . Kepko, L. (2008). Tail reconnection triggering substorm onset. *Science*, *321*, 931-935.
- Artemyev, A., Lu, S., El-Alaoui, M., Lin, Y., Angelopoulos, V., Zhang, X.-J., . . . Russell, C. (2021). Configuration of the earth's magnetotail current sheet. *Geophysical Research Letters*, *48*.

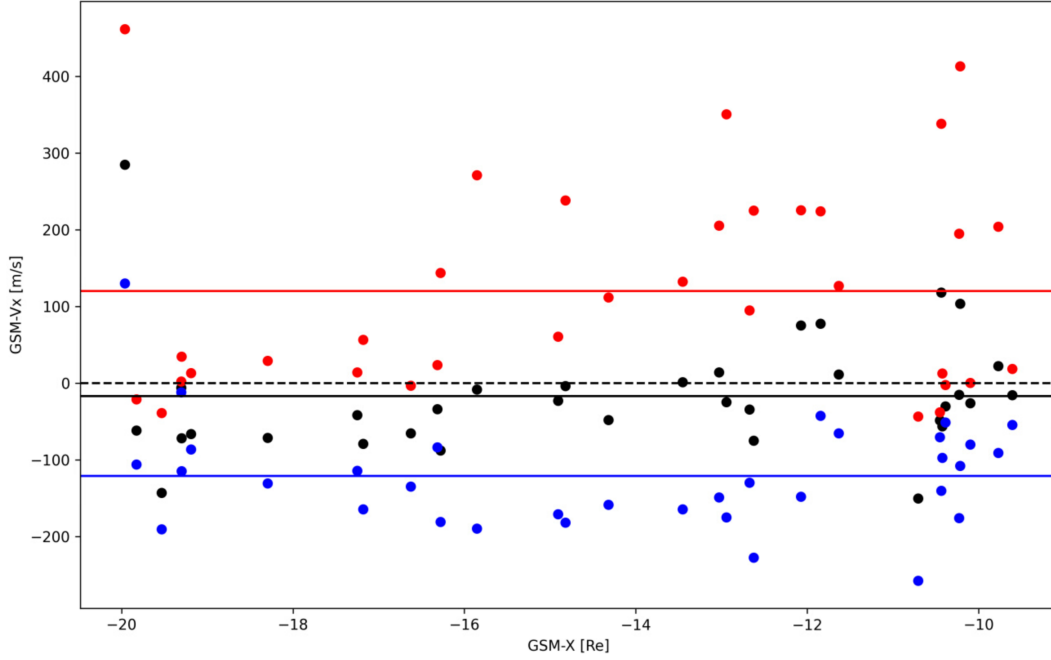


Figure A1. This shows the $V_{X,GSM}$ flow vs X_{GSM} position for all groups of x-lines identified within $20R_E$ of Earth in Run Mid. For each group we plot the maximum Earthward velocity (red), the mean velocity (black), and the minimum velocity (blue). The solid horizontal lines are the average of the maximum (red), mean (black), and minimum (blue) flows. The horizontal black and dashed line marks the difference between Earthward and tailward flows.

304 Baker, D., & P. (1996). Neutral line model of substorms: Past results and present
 305 view. *J. Geophys. Res.: Space Physics*, *101*, 12975-13010.
 306 Bard, C., & Dorelli, J. (2021). Magnetotail reconnection asymmetries in an ion-
 307 scale, earth-like magnetosphere. *Annales Geophysicae*, *39*, 991-1003.
 308 Bessho, N., & Bhattacharjee, A. (2014). Instability of the current sheet in the
 309 earth's magnetotail with normal magnetic field. *Physics of Plasmas*, *21*.
 310 Birn, J., & Hesse, M. (2013). The substorm current wedge in mhd simulations. *Jour-
 311 nal of Geophysical Research: Space Physics*, *118*, 3364-3376.
 312 Birn, J., Hesse, M., & Schindler, K. (1996). Mhd simulations of magnetotail dynam-
 313 ics. *J. Geophys. Res.*, *101*, 12939-12954.
 314 Birn, J., & Schindler, K. (2002). Thin current sheets in the magnetotail and the loss
 315 of equilibrium. *J. Geophys. Res.*, *107*.
 316 Coppi, B., Laval, G., & Pellat, R. (1966). Dynamics of the geomagnetic tail. *Physi-
 317 cal Review Letters*, *16*.
 318 El-Alaoui, M., Ashour-Abdalla, M., Walker, R., Perroomian, V., Richard, R., An-
 319 gelopoulos, V., & Runov, A. (2009). Substorm evolution as revealed by themis
 320 satellites and a globalmhd simulation. *Journal of Geophysical Research*, *114*.
 321 Gong, F., Yu, Y., & Cao, J. (2021). Simulating the responses of the magneto-
 322 sphere-ionosphere system to the imf by reversal. *Front. Phys.*, *10*.
 323 Hesse, M., & Birn, J. (1994). Mhd modeling of magnetotail instability for localized
 324 resistivity. *Journal of Geophysical Research*, *99*(A5), 8565-8576.
 325 Hesse, M., & Schindler, K. (2001). The onset of magnetic reconnection in the mag-
 326 netotail. *Earth, Planets and Space*, *53*, 645-653.
 327 Imber, S. M., Slavin, J. A., Auster, H. U., & Angelopoulos, V. (2022). A themis sur-
 328 vey of flux ropes and traveling compression regions: Location of the near-earth

- 329 reconnection site during solar minimum. *Journal Of Geophysical Research:*
 330 *Space Physics*, 116.
- 331 Liu, Y.-H., Birn, J., Daughton, W., Hesse, M., & Schindler, K. (2014). Onset of
 332 reconnection in the near magnetotail: Pic simulations. *Journal of Geophysical*
 333 *Research: Space Physics*, 119, 9773-9789.
- 334 Merkin, V. G., & Lyon, J. G. (2010). Effects of the low-latitude ionospheric bound-
 335 ary condition on the global magnetosphere. *Journal of Geophysical Research:*
 336 *Space Physics*, 115.
- 337 Merkin, V. G., Panov, E. V., Sorathia, K. A., & Ukhorskiy, A. Y. (2019). Contribu-
 338 tion of bursty bulk flows to the global dipolarization of the magnetotail during
 339 an isolated substorm. *Journal of Geophysical Research: Space Physics*, 124.
- 340 Min, K., Okuda, H., & Sato, T. (1985). Numerical studies on magnetotail formation
 341 and driven reconnection. *Journal of Geophysical Research: Space Physics*, 90,
 342 4035-4045.
- 343 Nagai, T., Fujimoto, M., Saito, Y., Machida, S., Terasawa, T., Nakamura, R., ...
 344 Kokubun, S. (1998). Structure and dynamics of magnetic reconnection for
 345 substorm onsets with geotail observations. *Journal of Geophysical Research:*
 346 *Space Physics*, 103, 4419-4440.
- 347 Nakamura, R., Baumjohann, W., Runov, A., Volwerk, M., Zhang, T. L., Klecker, B.,
 348 ... Frey, H. U. (2002). Fast flow during current sheet thinning. *Geophysical*
 349 *Research Letters*, 29.
- 350 Ohtani, S., Miyashita, Y., Singer, H., & Mukai, T. (2009). Tailward flows with posi-
 351 tive b_z in the near-earth plasma sheet. *Journal of Geophysical Research*, 114.
- 352 Panov, E. V., Nakamura, R., Baumjohann, W., Sergeev, V. A., Petrukovich, A. A.,
 353 Angelopoulos, V., ... Larson, D. (2010). Plasma sheet thickness during a
 354 bursty bulk flow reversal. *J. Geophys. Res.*, 115.
- 355 Park, K. (2021). Global mhd simulation of the weak southward imf condition for dif-
 356 ferent time resolutions. *Front. Astron. Space Sci.*, 8.
- 357 Pritchett, P. L. (2015). Structure of exhaust jets produced by magnetic reconnection
 358 localized in the out-of-plane direction. *Journal of Geophysical Research*, 120,
 359 592-608.
- 360 Raeder, J. (1999). Modeling the magnetosphere for northward interplanetary mag-
 361 netic field: Effects of electrical resistivity. *Journal of Geophysical Research:*
 362 *Space Physics*, 104.
- 363 Raeder, J. (2003). Global geospace modeling: Tutorial and review. space plasma
 364 simulation. *Lect. Notes Phys.*, 615, 212-246. (Edited by J. Büchner, C. Dum,
 365 and M. Scholer)
- 366 Raeder, J., Berchem, J., & Ashour-Abdalla, M. (1996). The importance of small
 367 scale processes in global mhd simulations: Some numerical experiments. *The*
 368 *Physics of Space Plasmas*, 14, 403. (Edited by T. Chang and j. R. Jasperse)
- 369 Raeder, J., McPherron, R. L., Frank, L. A., Paterson, W. R., Sigwarth, J. B., Lu,
 370 G., ... Slavin, J. A. (2001). Global simulation of the geospace environment
 371 modeling substorm challenge event. *J. Geophys. Res.*, 106.
- 372 Rogers, A. J., Farrugia, C. J., & Torbert, R. B. (2019). Numerical algorithm for
 373 detecting ion diffusion regions in the geomagnetic tail with applications to
 374 mms tail season 1 may to 30 september 2017. *Journal of Geophysical Research:*
 375 *Space Physics*, 124, 6487-6503.
- 376 Runov, A., Grandin, M., Palmroth, M., Battarbee, M., Ganse, U., Hietala, H., ...
 377 Turner, D. (2021). Ion distribution functions in magnetotail reconnection:
 378 global hybrid-vlasov simulation results. *Ann. Geophys.*, 39, 599-612.
- 379 Runov, A., Nakamura, R., Baumjohann, W., Zhang, T. L., Volwerk, M., Eichel-
 380 berger, H.-U., & Balogh, A. (2003). Cluster observation of a bifurcated current
 381 sheet. *Geophysical Research Letters*, 30.
- 382 Runov, A., Sergeev, V. A., Baumjohann, W., Nakamura, R., Apatenkov, S., Asano,
 383 Y., ... Rème, H. (2005). Electric current and magnetic field geometry in

- 384 flapping magnetotail current sheets. *Annales Geophysicae*, *23*, 1391-1403.
- 385 Runov, A., Sergeev, V. A., Nakamura, R., Baumjohann, W., Apatenkov, S., Asano,
- 386 Y., ... Balogh, A. (2006). Local structure of the magnetotail current sheet:
- 387 2001 cluster observations. *Annales Geophysicae*, *24*, 247-262.
- 388 Russell, C. T., & McPherron, R. L. (1973). The magnetotail and substorms. *Space*
- 389 *Sciences Reviews*, *15*, 205-266.
- 390 Schindler, K. (1974). A theory of the substorm mechanism. *Journal of Geophysical*
- 391 *Research: Space Physics*, *79*.
- 392 Scholer, M., & Otto, A. (1991). Magnetotail reconnection: Current diversion and
- 393 field-aligned currents. *Geophysical Research Letters*, *18*, 733-736.
- 394 Sergeev, V., Angelopoulos, V., Kubyshkina, M., Donovan, E., Zhou, X.-Z., Runov,
- 395 A., ... Nakamura, R. (2011). Substorm growth and expansion onset as ob-
- 396 served with ideal ground-spacecraft themis coverage. *Journal of Geophysical*
- 397 *Research: Space Physics*, *116*.
- 398 Sergeev, V., Runov, A., Baumjohann, W., Nakamura, R., Zhang, T. L., Volwerk, M.,
- 399 ... Klecker, B. (2003). Current sheet flapping motion and structure observed
- 400 by cluster. *Geophysical Research Letters*, *30*.
- 401 Sitnov, M. I., Buzulukova, N., Swisdak, M., Merkin, V. G., & Moore, T. E. (2013).
- 402 Spontaneous formation of dipolarization fronts and reconnection onset in the
- 403 magnetotail. *Geophysical Research Letters*, *40*.
- 404 Sitnov, M. I., & Schindler, K. (2010). Tearing stability of a multiscale magnetotail
- 405 current sheet. *Geophysical Research Letters*, *37*.
- 406 Sorathia, K. A., Merkin, V. G., Panov, E. V., Zhang, B., Lyon, J. G., & Garretson,
- 407 e. a., J. (2020). Ballooning-interchange instability in the near-earth plasma
- 408 sheet and auroral beads: Global magnetospheric modeling at the limit of the
- 409 mhd approximation. *Geophys. Res. Lett.*, *47*.
- 410 Stephens, G., Sitnov, M., Korth, H., Tsyganenko, N. A., Ohtani, S., Gkioulidou, M.,
- 411 & Ukhorskiy, A. Y. (2019). Global empirical picture of magnetospheric sub-
- 412 storms inferred from multimission magnetometer data. *Journal of Geophysical*
- 413 *Research: Space Physics*, *124*, 1085-1110.
- 414 Stephens, G. K., Sitnov, M. I., Weigel, R. S., Turner, D. I., Tsyganenko, N. A.,
- 415 Rogers, A. J., ... Slavin, J. A. (2022). Global structure of magnetotail recon-
- 416 nection revealed by mining space magnetometer data. *Earth and Space Science*
- 417 *Open Archive*. doi: 10.1002/essoar.10511996.1
- 418 Torbert, R. B., Burch, J. L., Phan, T. D., Hesse, M., Argall, M. R., Shuster, J., &
- 419 Ergun, R. E. e. a. (2018). Electron-scale dynamics of the diffusion region
- 420 during symmetric magnetic reconnection in space. *Science*, *362*, 1391-1395.
- 421 Ugai, M., & Tsuda, T. (1979). Magnetic field-line reconexion by localized enhance-
- 422 ment of resistivity. part 4. dependence on the magnitude of resistivity. *Journal*
- 423 *of Plasma Physics*, *22*, 1-14.
- 424 Zhang, B., Sorathia, K., Lyon, J., Merkin, V., Garretson, J., & Wiltberger, M.
- 425 (2019). Gamera: A three-dimensional finite-volume mhd solver for non-
- 426 orthogonal curvilinear geometries. *The Astrophysical Journal*, *244*.
- 427 Zhang, L. Q., Liu, Z. X., Ma, Z. W., Baumjohann, W., Pu, Z. Y., Dunlop, M. W.,
- 428 ... Wang, J. Y. (2010). X line distribution determined from earthward and
- 429 tailward convective bursty flows in the central plasma sheet. *Journal of Geo-*
- 430 *physical Research*, *115*.
- 431 Zhao, S., Tian, A., Shi, Q., Xizo, C., Fu, S., Zong, Q., ... Tan, K. (2016). Statistical
- 432 study of magnetotail flux ropes near the lunar orbit. *Science China Technologi-*
- 433 *cal Sciences*, *59*, 1591-1596.